

# Analysing the response in R2\* relaxation rate of intracranial tumours to hyperoxic and hypercapnic respiratory challenges: initial results

A. Müller · S. Remmele · I. Wenningmann ·  
H. Clusmann · F. Träber · S. Flacke · R. König ·  
J. Gieseke · W. A. Willinek · H. H. Schild · P. Mürtz

Received: 6 July 2010 / Accepted: 8 August 2010 / Published online: 22 September 2010  
© European Society of Radiology 2010

## Abstract

**Objective** To investigate the response in R2\* relaxation rate of human intracranial tumours during hyperoxic and hypercapnic respiratory challenges.

**Methods** In seven patients with different intracranial tumours, cerebral R2\* changes during carbogen and CO<sub>2</sub>/air inhalation were monitored at 3 T using a dynamic multigradient-echo sequence of high temporal and spatial resolution. The R2\* time series of each voxel was tested for

significant change. Regions of interest were analysed with respect to response amplitude and velocity.

**Results** The tumours showed heterogeneous R2\* responses with large interindividual variability. In the ‘contrast-enhancing’ area of five patients and in the ‘non-tumoral’ tissue most voxels showed a decrease in R2\* for carbogen. For the ‘contrast-enhancing’ area of two patients hardly any responses were found. In areas of ‘necrosis’ and perifocal ‘oedema’ typically voxels with R2\* increase and no response were found for both gases. For tissue responding to CO<sub>2</sub>/air, the R2\* changes were of the same order of magnitude as those for carbogen. The response kinetic was generally attenuated in tumoral tissue.

**Conclusion** The spatially resolved determination of R2\* changes reveals the individual heterogeneous response characteristic of intracranial human tumours during hyperoxic and hypercapnic respiratory challenges.

A. Müller · F. Träber · R. König · J. Gieseke · W. A. Willinek ·  
H. H. Schild · P. Mürtz (✉)  
Department of Radiology, University of Bonn,  
Sigmund-Freud-Straße 25,  
53105 Bonn, Germany  
e-mail: petra.muertz@ukb.uni-bonn.de

S. Remmele  
Philips Research Europe,  
Hamburg, Germany

I. Wenningmann  
Department of Anesthesiology and Intensive Care Medicine,  
University of Bonn,  
Bonn, Germany

H. Clusmann  
Department of Neurosurgery, University of Bonn,  
Bonn, Germany

S. Flacke  
Department of Radiology, Lahey Clinic,  
Tufts University Medical School,  
Burlington, MA, USA

J. Gieseke  
Philips Healthcare,  
Best, The Netherlands

**Keywords** MRI · Intracranial tumour · R2\* relaxation rate quantification · Oxygenation · Vasoreactivity

## Introduction

Magnetic resonance imaging (MRI) accurately displays anatomical structures of intracranial tumours. Diffusion tensor and perfusion MRI provide information on cell density, tumour infiltration [1, 2], blood volume/flow and vascular permeability [3, 4]. Novel positron emission tomography (PET) techniques aim to determine the degree of hypoxia and cellular proliferation [5–7]. The image based assessment of tumour tissue oxygenation and angiogenesis, which could directly impact treatment planning and monitoring, is still matter of research [8–12].

Blood oxygenation level-dependent (BOLD) MRI in combination with hyperoxic and hypercapnic respiratory challenges [13] offers a non-invasive approach to assess tumour oxygenation and vasoreactivity without exposure to ionising radiation. BOLD MRI uses deoxyhaemoglobin (dHb) as an endogenous contrast agent. dHb's paramagnetic nature shortens the apparent spin-spin relaxation time  $T2^*$ , which can be assessed by using gradient-echo sequences. Unfortunately, baseline  $T2^*$  is also affected by static tissue components such as iron content and large-scale susceptibility gradients at tissue interfaces. However, changes in the relaxation rate  $R2^*$  ( $=1/T2^*$ ) correlate directly with changes in the dHb content [10, 14]. The venous dHb content of a voxel can be modulated by respiratory challenges, which change blood oxygenation saturation and cerebral blood flow/volume. Inhalation of carbogen (5%  $CO_2$  in  $O_2$ ) or  $CO_2$ /air (5%  $CO_2$  in air) can decrease  $R2^*$  of healthy cerebral tissue [15] without changing the cerebral metabolic rate of oxygen [16]. Such measurements lead to information on oxygenation changes [10–12, 17, 18] and vasoreactivity [19–26]. In tumours, these parameters give an insight into vessel functionality (erythrocyte perfusion) and maturity [27, 28]. The potential of this method is underlined by numerous animal [17, 18, 27–35] and first human tumour studies [36–42].

Commonly, the response to respiratory challenges is determined by measuring signal changes in  $T2^*$ -weighted gradient-echo images acquired at a single echo time [36–38, 41, 42]. However, this approach doesn't provide quantitative data and fails to eliminate influences of the apparent longitudinal relaxation rate  $R1^*$ . Changes in the content of dissolved oxygen and in inflow effects induced by respiratory challenges may affect  $R1$  and thus the resulting images [16]. Furthermore, data acquired at a single echo time will only provide accurate measurements for a small range of  $R2^*$  values. Tumours are heterogeneous with a broad range of  $R2^*$  values. The determination of  $R2^*$  obtained from multigradient-echo data overcomes these limitations. Until now, studies on  $R2^*$  quantification during respiratory challenges in human brain have been scarce [15, 22, 39].

For intracranial tumours, no voxel-wise analysis of  $R2^*$  changes has been reported as yet.

The aims of our work were the spatially resolved determination of  $R2^*$  changes during respiratory challenges in human intracranial tumours, and to perform a tissue-specific response analysis. Carbogen and  $CO_2$ /air were used in order to obtain separate information on oxygenation and vasoreactivity.

## Methods

### Study population

Seven patients (aged 31–74 years) with various intracranial tumours and no signs of elevated intracranial pressure were included in the study (see Table 1). Tumour types were confirmed histologically in all cases except for one patient with metastasis of lung cancer. The institutional review board approved this study. Written informed consent was obtained from all patients.

### MRI protocol

Magnetic resonance (MR) imaging was performed with a 3 T whole-body system (Achieva, Philips Healthcare, Best, The Netherlands; Quasar Dual gradient system: 80 mT/m maximum amplitude, 0.16 ms minimal rise time, 200 T/m/s maximum slew rate) using a transmit/receive quadrature head coil.

For  $R2^*$  quantification during the respiratory challenge, a dynamic multigradient-echo (MGE) echo-planar-imaging (EPI) sequence (see Table 2) with high temporal and spatial resolution (198 dynamic frames, 2.13 s/frame, voxel size of  $1.8 \times 1.8 \times 5 \text{ mm}^3$ ) was used to measure one single transverse slice located through the largest tumour extent. This multi-shot variant reduced susceptibility artefacts and allowed for a smaller minimum TE value and a higher spatial resolution without decreasing the signal-to-noise ratio. High-order volume shimming was used to achieve high  $B_0$  homogeneity.

**Table 1** Overview of all patients examined in this study

Patient	Gender	Age	Tumour type
P1	m	31	Meningioma, WHO grade I
P2	m	74	Meningioma, WHO grade II with infiltration to the brain
P3	w	53	Glioblastoma multiforme, WHO grade IV
P4	m	69	Glioblastoma multiforme, WHO grade IV
P5	w	56	Metastasis of bronchial carcinoma
P6	w	56	Metastasis of bronchial carcinoma
P7	w	60	Non-Hodgkin's lymphoma

**Table 2** Sequence parameters list

	T2* MGE (multi-shot)	T2 TSE	DTI SE-EPI (single-shot)	CASL (single-shot)	T1 CE
FOV	230×201 axial	230×184 axial	230×230 axial	230x230 axial	230x183 axial
TE/TR	4.0–83.2/97 ms (12 echoes in steps of 7.2 ms)	80/3673 ms	56/2700 ms	31/4500 ms	13/550 ms
Flip angle	25°	90°	90°	90°	90°
Number of slices	1	23	11	11	24
Turbo/EPI factor	–/5	16/–	–/127	–/63	–/–
Fat suppression	SPIR	–	SPIR	SPIR	–
Pixel bandwidth	1290 Hz in EPI frequ. dir.	175 Hz	2818 Hz in EPI frequ. dir.	4388 Hz in EPI frequ. dir.	174 Hz
Voxel size	1.8×1.8×5 mm	0.6×0.7×5 mm	1.8×1.8×5 mm	3.6x3.6x5 mm	0.9x1.1x5 mm
# Averages	1	1	2 for b0, 6 for bmax	1	1
# Dynamics	198+10 dummies	–	–	30	–
Specials	–	–	b0/bmax=0/1600 s/mm <sup>2</sup> 6 non-collinear directions $\delta/\Delta=11.0/27.5$ ms	labelling duration/ post-labelling delay: 2200/1000 ms	–
Acquisition time	7:02+0:21 min	2:05 min	1:48 min	5:24 min	3:03 min

The following abbreviations were used: *MGE* multigradient-echo, *TSE* turbo spin echo, *SE* spin echo, *CASL* continuous arterial spin labelling, *SPIR* spectral presaturation by inversion recovery, *EPI* echo-planar-imaging, *CE* contrast-enhanced,  $\delta/\Delta$ —duration/distance of diffusion gradients, # number. The EPI factor denotes the number of k-space profiles collected per excitation

The examination protocol (for details see Table 2) also contained a T2-weighted turbo spin echo sequence, a diffusion tensor imaging (DTI) sequence, and a continuous arterial spin-labelling (CASL) perfusion sequence. Gadolinium-DTPA (0.10 mmol per kg body weight, Magnevist, Schering, Berlin, Germany) contrast-enhanced T1-weighted spin echo images were acquired (for patients P1, P3, P4, P7) if not available from a previous examination. Maps of the apparent diffusion coefficient (ADC) and the fractional anisotropy (FA) as well as perfusion-weighted images (mean of the dynamic label minus control images) were generated at the MRI console (manufacturer supplied application software, release 3.1.1.0).

#### Breathing protocol

Carbogen (95%O<sub>2</sub>/5%CO<sub>2</sub>) and CO<sub>2</sub>/air (5%CO<sub>2</sub>/25%O<sub>2</sub>/70%N<sub>2</sub>), both delivered by Linde, Unterschleissheim, Germany, were used to induce hypercapnic hyperoxia and hypercapnia, respectively, following a protocol of 1/4/2 min of air/gas/air inhalation. The breathing system consisted of a tightly fitting breathing mask, a two-way valve, and two flexible tubes for the inspiratory and expiratory air stream. The inhalation gases were supplied via a demand valve (Oxidem 3000, Dräger, Lübeck, Germany), allowing high breathing gas volumes per inhalation.

Throughout the experiments, the inspired oxygen fraction (F<sub>i</sub>O<sub>2</sub>), the inspired and end-tidal CO<sub>2</sub> partial pressures (P<sub>i</sub>CO<sub>2</sub> and P<sub>et</sub>CO<sub>2</sub>, respectively), and the breathing rate were continuously measured at the mask (Magnitude<sup>TM</sup> 3150/3155, Invivo, Orlando, FL, USA,

measurement accuracy of ±4 mmHg for CO<sub>2</sub> and ±5% for O<sub>2</sub>, calibration of the capnometer was checked before each examination). Pulse rate and blood pressure were also recorded.

#### Multigradient-echo data processing

The processing of the MGE data was done offline using custom-built research software (Philips Research Europe, Hamburg, Germany) based on IDL 6.3 (Research Systems, Inc., Boulder, CO, USA). Motion correction,  $\Delta R2^*$  quantification and response analysis were performed as previously described [15]. In short, the R2\* values were obtained from monoexponential decay functions. The R2\* change at each dynamic step *i*,  $\Delta R2^*_i$ , was calculated in relation to a reference value. Voxels with significantly changed R2\* values were identified by performing a Student's *t*-test ( $p < 0.05$ , unequal variance) and comparing the  $\Delta R2^*_i$  values acquired during the respiratory challenge with those acquired during breathing room air (baseline data). Translational periods of 60 s after changing the inhalation gas were excluded from analysis. Voxels with significant response were displayed on a colour-coded overlay map.

#### Modelling the R2\* response

For quantitative analysis of the response within a region of interest (ROI), the  $\Delta R2^*_i$  time series from all voxels with a significant R2\* change were averaged, separately for negative and positive responses. These two response functions  $\Delta R2^*_i$  were further corrected for linear drifts of

the baseline data and approximated by a monoexponential model function [43]:

$$Response(t) = \begin{cases} 0 & t < t_1 \\ A (1 - e^{-(t-t_1)/\tau_1}) & t_1 \leq t < t_2 \\ A (1 - e^{-(t_2-t_1)/\tau_1}) e^{-(t-t_2)/\tau_2} & t_2 \leq t \end{cases} \quad (1)$$

By using a non-linear least-squares fit (Levenberg-Marquardt), the maximum change A, the time constants  $\tau_1$  and  $\tau_2$  of the changes, and the start and end points  $t_1$  and  $t_2$  of the induced response were determined. The fit quality was indicated by the coefficient of determination  $R^2$  (i.e.  $1 - [\text{residual sum of squares}]/[\text{data variance}]$ ).

ROI-based R2\* response analysis

The R2\* response was further analysed in different ROIs within the tumour and also in surrounding ‘non-tumoral’ tissue:

- (T) ‘contrast-enhancing’ tumour area,
- (N) ‘necrotic’ tumour area characterised by central hypointensity within the ‘contrast-enhancing’ tumour and clear hyperintensity on the ADC map (small focal regions were not considered),
- (E) area considered as perifocal ‘oedema’ with T2 hyperintensity, no contrast enhancement, and a slight hyperintensity on the ADC map, and
- (X) ‘non-tumoral’ tissue comprising cerebral tissue with normal appearance on T2-weighted images far away from the tumour, not including ventricles, deep cerebral veins and sinuses.

For each ROI, the following analysis was performed:

- a) the numbers of voxels with decreased, increased and unchanged R2\* values were determined from the *t*-test,
- b) the response functions were analysed for maximum change A,  $\tau_1$  and  $\tau_2$ , and fit quality  $R^2$ .

**Fig. 1** R2\* response of human tumours. From left to right the T2-weighted images T2 TSE, the contrast agent-enhanced T1-weighted images T1 CE (with the exception of patient P5, where the subtraction of the T1 CE and T1 images is given), the ADC maps, the R2\* maps of the first dynamic (during air breathing), and the overlay maps of significant R2\* changes ( $\Delta R2^*$ ) during carbogen and CO<sub>2</sub>/air inhalation are displayed for all examined patients (see Table 1). ‘T’, ‘N’, ‘E’ and ‘X’ denote the defined ROIs in the ‘contrast-enhancing’ tumour area, ‘necrosis’, ‘oedema’, and ‘non-tumoral’ tissue, respectively. Voxels with significant R2\* decrease ( $\Delta R2^* < 0$ ) and increase ( $\Delta R2^* > 0$ ) are displayed colour-coding (white to red and light blue to dark blue, respectively). The colours scale linearly with the mean difference between the baseline and response data used in the *t*-test ( $p=0.05$ ). The underlying images are peak height images (sum of all echoes) of the first dynamic. Two different responses are seen in meningioma. A well-perfused meningioma (WHO I°, P1) shows a decrease in R2\* for both gases whereas a hypoperfused meningioma (WHO II°, P2) displays no change or minimal increase in R2\* likely related to a low density of functional vessels and a lack of normal vasoreactivity. A decrease in R2\* for both gases indicating good vascularisation and ‘normal’ vasoreactivity is seen in the ring-shaped well perfused enhancing tumour area in a glioblastoma (P4) and a metastasis (P5). Mixed responses to CO<sub>2</sub>/air are found in the ‘contrast-enhancing’ tumour area of another glioblastoma (P3). The necrotic centre of the lesions and the perifocal ‘oedema’ reveal typically voxels with increased or unchanged R2\* values for both gases

- c) the predominant kind of R2\* response as obtained in a) was compared with the perfusion status, which was graded by two experienced readers in consensus as ‘hyper-’, ‘iso-’, or ‘hypoperfused’ compared with a corresponding area in the contralateral hemisphere.

Results

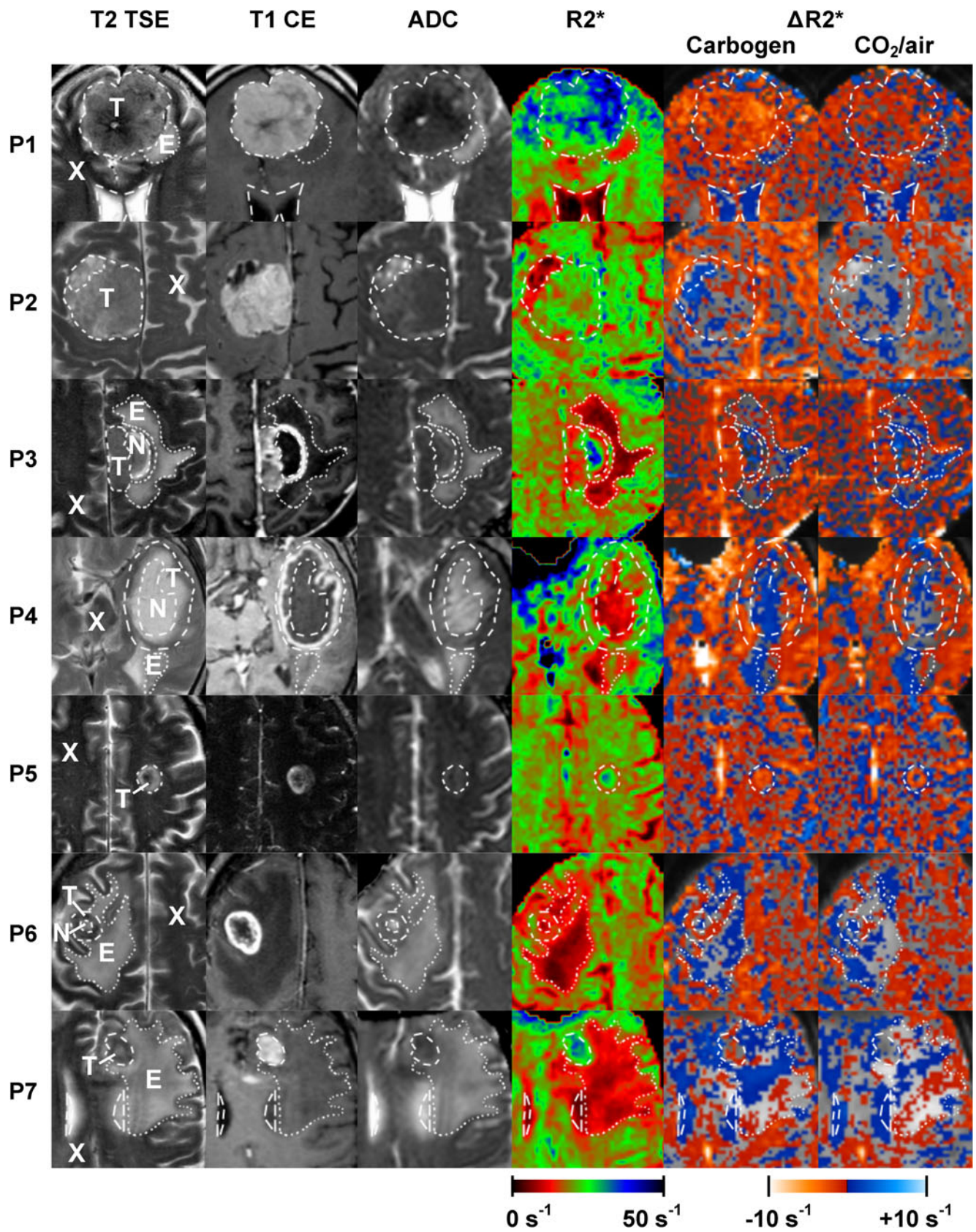
Physiological parameters

The breathing of the CO<sub>2</sub>-enriched gases was well tolerated by all patients. The physiological parameters are summarised in Table 3. F<sub>i</sub>O<sub>2</sub> and P<sub>i</sub>CO<sub>2</sub> values confirmed the tightness of the breathing system. P<sub>et</sub>CO<sub>2</sub>, being a rough measure for arterial P<sub>a</sub>CO<sub>2</sub> [44], was significantly changed ( $p < 0.001$ , pairwise Student’s *t*-test) by  $13 \pm 3$  mmHg for carbogen and by  $16 \pm 3$  mmHg for CO<sub>2</sub>/air.

**Table 3** Physiological parameters

	<i>n</i> =7	Air	Carbogen	Air	CO <sub>2</sub> /air
All values given as mean and standard deviation over all seven patients were measured during the steady state condition. F <sub>i</sub> O <sub>2</sub> , P <sub>i</sub> CO <sub>2</sub> and P <sub>et</sub> CO <sub>2</sub> changed significantly ( $p < 0.001$ , pairwise Student’s <i>t</i> -test) during gas inhalation. Changes in P <sub>et</sub> CO <sub>2</sub> differed significantly under both conditions ( $p < 0.001$ , pairwise Student’s <i>t</i> -test)					
Pulse rate [min <sup>-1</sup> ]		59±6	59±7	59±6	59±6
Blood pressure systolic [mmHg]		136±14	151±15	136±22	151±19
Blood pressure diastolic [mmHg]		74±10	83±14	76±14	80±12
Respiration rate [min <sup>-1</sup> ]		15±5	16±5	16±4	16±5
F <sub>i</sub> O <sub>2</sub> [%]		19±1	93±1	20±1	24±1
P <sub>i</sub> CO <sub>2</sub> [mmHg]		1±1	37±1	0±1	38±2
P <sub>et</sub> CO <sub>2</sub> [mmHg]		37±5	49±3	34±4	50±3
P <sub>et</sub> CO <sub>2</sub> (gas)- P <sub>et</sub> CO <sub>2</sub> (air) [mmHg]			13±3		16±3





R2\* response maps

All T<sub>2</sub>\*-weighted images were of good quality with respect to motion and susceptibility artefacts. Figure 1 displays the results of R2\* response mapping as obtained from the voxel-wise *t*-test of the dynamic R2\* series. In ‘non-tumoral’ tissue, the strongest R2\* decrease occurred in and around cerebral sulci, where voxels contain veins and/or grey matter with a high blood volume. R2\* changes within the superior sagittal sinus were found to be between -19 s<sup>-1</sup> and -31 s<sup>-1</sup> for carbogen and between -13 s<sup>-1</sup> and -27 s<sup>-1</sup> for CO<sub>2</sub>/air. The lowest R2\* changes were found in white matter, where negative and positive changes of up to ±0.5 s<sup>-1</sup> were detected. Small positive changes were also detected in the ventricles and partly in the sulci. Response patterns differed between tumour entities and specific areas within each tumour.

ROI-based R2\* response analysis

Table 4 summarises the fractions of negatively, positively and non-responding voxels for the investigated ROIs. ‘Non-tumoral’ tissue showed predominantly negative R2\* changes for carbogen in all cases and in 5/7 cases also for CO<sub>2</sub>/air. The

amount of voxels with increased R2\* was less than 32% in all cases. In the ‘contrast-enhancing’ tumour area negative R2\* changes were observed in 5/7 and 4/7 patients for carbogen and CO<sub>2</sub>/air, respectively. One hypoperfused meningioma (P2) and one lymphoma (P7) hardly responded to either of the two challenges. A larger metastasis (P6) was only sensitive to carbogen. Areas of ‘necrosis’ and perifocal ‘oedema’ (with the exception of P1) showed voxels with increased or unchanged R2\* values for both respiratory challenges regardless of tumour histology. Generally, the response in tumour tissue was more heterogeneous than in ‘non-tumoral’ tissue and the spatial distribution of R2\* changes within the tumour varied between subjects.

Results for the ROI response functions are given in Table 5, a typical plot of the temporal behaviour for different ROIs is given in Fig. 2. Comparing the two gases, it was found, that the observed changes were of the same order of magnitude but with partially different characteristics. For ‘non-tumoral’ tissue negative changes between -1.1 and -2.2 s<sup>-1</sup> were found for both gases, with the exception of patient P2 (hypoperfused meningioma), in whom a large R2\* decrease of -3.3 s<sup>-1</sup> during carbogen was found. For ‘contrast-enhancing’ tumour areas, patients with a

**Table 4** Region-of-interest analysis concerning the number of voxels with decreased, increased and unchanged R2\* values as a result of the *t*-test

Patient	Vital tumour (T)				Necrosis (N)				Oedema (E)				Non-tumoral tissue (X)			
	#vox	n [%]	p [%]	ns [%]	#vox	n [%]	p [%]	ns [%]	#vox	n [%]	p [%]	ns [%]	#vox	n [%]	p [%]	ns [%]
a)																
P1	432	85	6	9					74	45	24	31	3191	59	16	25
P2	437	26	30	43									1951	58	13	29
P3	86	94	1	5	76	17	34	49	228	25	18	56	2878	67	8	24
P4	351	60	19	21	178	14	67	19	71	20	51	30	1535	63	12	24
P5	52	71	19	10									3624	52	27	21
P6	43	63	2	35	8	0	50	50	292	4	55	41	2226	54	20	26
P7	51	43	4	53					468	18	46	36	2561	48	22	30
MW		63	12	25		10	51	39		22	39	39		57	17	26
STD		23	11	19		9	17	18		15	16	11		7	6	3
b)																
P1	432	58	12	30					74	16	42	42	3191	48	19	33
P2	437	11	22	67									1951	38	12	50
P3	86	49	19	33	76	28	45	28	228	22	38	40	2878	47	21	32
P4	351	50	16	33	178	13	35	52	71	27	42	31	1535	49	17	34
P5	52	48	40	12									3624	47	32	21
P6	43	23	16	60	8	0	100	0	292	7	38	55	2226	51	19	30
P7	51	8	20	73					468	24	23	53	2561	34	25	41
MW		35	21	44		14	60	26		19	37	44		45	21	34
STD		21	9	23		14	35	26		8	8	10		6	6	9

For the defined ROIs (Fig. 1) in each patient (Table 1), the total number of voxels (#vox) and the fractions of negatively (n), positively (p) and non-significantly (ns) changed voxels are summarised for a) carbogen and b) CO<sub>2</sub>/air. The mean values (‘MW’) and their standard deviations (‘STD’) are also given

**Table 5** Results obtained by parameterisation of the ‘global’ ROI response function

Patient	Vital tumour (T)				Necrosis (N)				Oedema (E)				Non-tumoral tissue (X)			
	$A_p$ [s <sup>-1</sup> ]	$\tau_{1_p}$ [s]	$\tau_{2_p}$ [s]	$R^2_p$	$A_n$ [s <sup>-1</sup> ]	$\tau_{1_n}$ [s]	$\tau_{2_n}$ [s]	$R^2_n$	$A_e$ [s <sup>-1</sup> ]	$\tau_{1_e}$ [s]	$\tau_{2_e}$ [s]	$R^2_e$	$A_x$ [s <sup>-1</sup> ]	$\tau_{1_x}$ [s]	$\tau_{2_x}$ [s]	$R^2_x$
a)																
P1	-3.4	130	34	<b>0.90</b>					-1.9	21	97	<b>0.60</b>	-1.4	18	14	<b>0.97</b>
P2	-1.7	88	46	0.24									-3.3	87	28	<b>0.54</b>
P3	-1.6	34	16	<b>0.88</b>	-1.7	68	38	0.35	-0.6	4	3	0.34	-2.2	51	23	<b>0.98</b>
P4	-2.0	43	29	<b>0.73</b>	-1.8	96	40	0.38	-1.3	185	20	0.17	-1.6	33	18	<b>0.96</b>
P5	-2.5	44	76	<b>0.79</b>									-1.8	18	63	<b>0.95</b>
P6	-1.5	86	15	<b>0.18</b>					-1.1	79	22	0.35	-1.7	31	8	<b>0.92</b>
P7	-1.0	14	16	0.29					-0.5	25	17	0.25	-1.2	30	17	<b>0.96</b>
MW	-2.0	63	33	0.57	-1.7	82	39	0.36	-1.1	63	32	0.34	-1.9	38	24	0.90
STD	0.8	40	22	0.32	0.0	20	1	0.02	0.6	74	37	0.16	0.7	24	18	0.16
b)																
P1	-2.4	145	14	<b>0.69</b>	-0.7	1	3	0.41					-1.2	71	20	<b>0.93</b>
P2	-1.2	6	1	0.22									-1.7	49	37	0.40
P3	-1.3	55	15	<b>0.71</b>	-2.0	52	27	0.65	-1.2	74	38	0.72	-2.1	65	37	<b>0.96</b>
P4	-2.2	91	36	<b>0.65</b>	-1.7	86	20	0.42	-0.9	40	1	0.17	-1.5	55	17	<b>0.85</b>
P5	-3.5	118	24	<b>0.84</b>									-2.0	68	30	<b>0.95</b>
P6	-1.5	72	4	0.20					-0.6	32	19	0.14	-1.5	86	14	<b>0.86</b>
P7	-0.9	32	26	0.10					-0.5	31	9	0.25	-1.1	52	23	0.94
MW	-1.9	74	17	0.49	-1.9	69	24	0.54	-0.8	36	14	0.34	-1.6	64	25	0.84
STD	0.9	48	12	0.30	0.2	24	5	0.17	0.3	26	15	0.24	0.4	13	9	0.20
Patient	Vital tumour (T)				Necrosis (N)				Oedema (E)				Non-tumoral tissue (X)			
	$A_p$ [s <sup>-1</sup> ]	$\tau_{1_p}$ [s]	$\tau_{2_p}$ [s]	$R^2_p$	$A_n$ [s <sup>-1</sup> ]	$\tau_{1_n}$ [s]	$\tau_{2_n}$ [s]	$R^2_n$	$A_e$ [s <sup>-1</sup> ]	$\tau_{1_e}$ [s]	$\tau_{2_e}$ [s]	$R^2_e$	$A_x$ [s <sup>-1</sup> ]	$\tau_{1_x}$ [s]	$\tau_{2_x}$ [s]	$R^2_x$
a)																
P1	1.2	16	15	0.64					1.2	50	14	0.49	0.8	11	30	0.76
P2	1.6	8	1	0.31									1.4	10	4	0.35
P3	0.9	29	3	0.15	1.6	9	1	0.44	0.6	4	3	0.46	1.3	25	20	0.83
P4	1.2	72	20	0.28	<b>1.6</b>	<b>76</b>	<b>21</b>	<b>0.28</b>	<b>2.0</b>	<b>138</b>	<b>19</b>	<b>0.24</b>	1.0	97	39	0.42
P5	1.2	10	43	0.62									1.7	12	45	0.93
P6	0.5	38	14	0.01	<b>1.3</b>	<b>61</b>	<b>17</b>	<b>0.02</b>	<b>0.9</b>	<b>62</b>	<b>20</b>	<b>0.18</b>	2.0	116	19	0.65
P7	0.7	2	25	0.24					<b>1.1</b>	<b>52</b>	<b>25</b>	<b>0.37</b>	1.0	45	13	0.36
MW	1.1	25	17	0.32	1.5	49	13	0.25	1.2	61	16	0.34	1.3	45	24	0.61
STD	0.4	24	14	0.23	0.2	35	11	0.21	0.5	48	8	0.13	0.4	44	15	0.24



**Table 5** (continued)

Patient	Vital tumour (T)				Necrosis (N)				Oedema (E)				Non-tumoral tissue (X)			
	A_p [s <sup>-1</sup> ]	τ <sub>1_p</sub> [s]	τ <sub>2_p</sub> [s]	R <sup>2</sup> _p	A_p [s <sup>-1</sup> ]	τ <sub>1_p</sub> [s]	τ <sub>2_p</sub> [s]	R <sup>2</sup> _p	A_p [s <sup>-1</sup> ]	τ <sub>1_p</sub> [s]	τ <sub>2_p</sub> [s]	R <sup>2</sup> _p	A_p [s <sup>-1</sup> ]	τ <sub>1_p</sub> [s]	τ <sub>2_p</sub> [s]	R <sup>2</sup> _p
b) P1	1.3	75	17	0.45					1.6	145	3	0.37	1.0	67	29	0.72
P2	1.1	44	30	0.07					1.0	66	30	0.69	1.2	1	1	0.19
P3	0.8	33	83	0.38	2.2	34	49	0.71	1.0	16	1	0.08	1.4	36	17	0.91
P4	1.3	58	28	0.66	1.2	4	1	0.22	1.0	16	1	0.08	1.0	38	25	0.29
P5	0.9	38	20	0.39					0.9	56	38	0.32	2.1	81	37	0.86
P6	1.0	28	20	0.04	1.5	75	51	0.08	0.9	23	3	0.14	2.1	108	28	0.63
P7	0.7	23	5	0.28					0.6	61	15	0.32	0.9	41	24	0.22
MW	1.0	43	29	0.33	1.7	38	34	0.34	1.0	51	18	0.24	1.4	53	23	0.54
STD	0.2	18	25	0.22	0.5	36	28	0.33	0.4	51	18	0.24	0.5	35	11	0.31

The maximum change A, the time constants τ<sub>1</sub> and τ<sub>2</sub>, and the fit quality R<sup>2</sup> in the case of negative and positive R2\* responses (indicated by ‘n’ and ‘p’, respectively) to a) carbogen and b) CO<sub>2</sub>/air are summarised for the ROIs defined (Fig. 1) in each patient (Table 1). The predominant response is marked by bold letters. The mean values (‘MW’) and their standard deviations (‘STD’) are also given for rough comparison

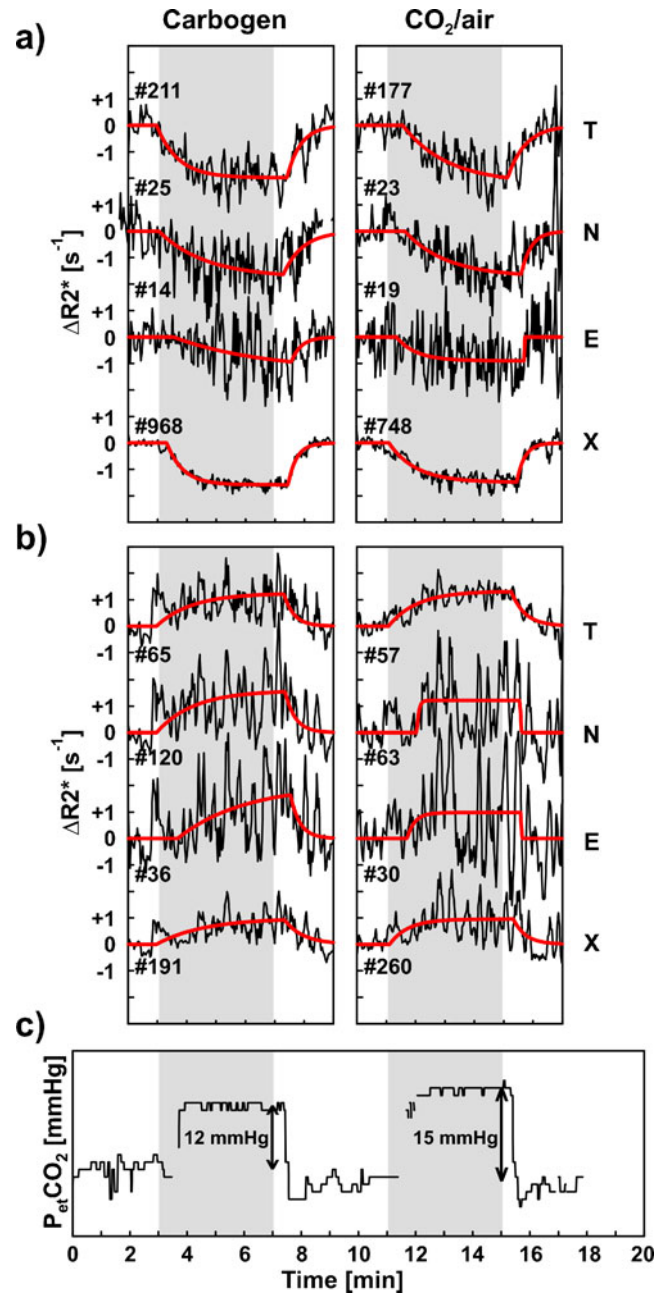


**Fig. 2** Typical ROI response functions for a) negative and b) positive changes in R2\* (patient 4). For ROI positions see Fig. 1 and for corresponding fit results Table 5. The number of significantly negatively/positively changed voxels included as well as the P<sub>et</sub>CO<sub>2</sub> course (c) are also given

large negative R2\* change (−3.4 s<sup>-1</sup> for P1 under carbogen and −3.5 s<sup>-1</sup> for P5 under CO<sub>2</sub>/air), patients with a medium-sized change (similar to that in ‘non-tumoral’ tissue) as well as patients with a small change (for the lymphoma P7) were found. The positive R2\* changes in ‘necrotic’ areas and ‘oedemas’ were between +0.9 and +2.2 s<sup>-1</sup>.

R2\* changes during the respiratory challenges were slower than during normalisation. Tumour had longer and



more variable time constants  $\tau_1$  and  $\tau_2$  (of up to 184 and 97 s, respectively) compared with ‘non-tumoral’ tissue.

The negative response functions of ‘non-tumoral’ tissue and of ‘contrast-enhancing’ tumour areas were very well presented by the monoexponential model (high fit quality). In ‘necrosis’ and ‘oedemas’ as well as in positively changed areas of ‘contrast-enhancing’ tumour and ‘non-tumoral’ tissue the fit quality was low. In some of these ROIs it was difficult to reach any fit with  $R^2 > 0$  (Fig. 2b). In order to check whether a bad fit quality was caused by averaging of the voxel-wise time series of different behaviour, a voxel-wise response modelling was also performed (see Fig. 3). On the map displaying the fit quality wide areas exhibit low fit quality. Setting the threshold for  $R^2$  to 0.05, a similar number of responsive voxels can be found as for the  $t$ -test with  $p=0.05$ . In general, changes displayed on the A-maps are larger than those on the corresponding  $\Delta R2^*$  maps, because in the  $\Delta R2^*$  maps the average change during the last three minutes of respiratory challenge is given, whereas

in the A-map the maximum expected changes assuming a monoexponential model function are given. White spots on the A-maps indicate outliers. The principal pattern of the changes looks very similar on both maps.

Tables 6 and 7 compares the degree of perfusion with the detected response behaviour. All of the hyperperfused areas responded with a predominant decrease in  $R2^*$  during both respiratory challenges. In isoperfused and hypoperfused areas, no consistent  $R2^*$  response was found.

## Discussion

The MRI response of human intracranial tumours during respiratory challenges has been previously investigated at 1.5 T using either signal changes [37, 45] or  $T2^*$  changes within regions of interest [39]. To our knowledge, this is the first study to provide a spatially resolved  $R2^*$  response analysis. We used a dynamic multigradient-echo sequence

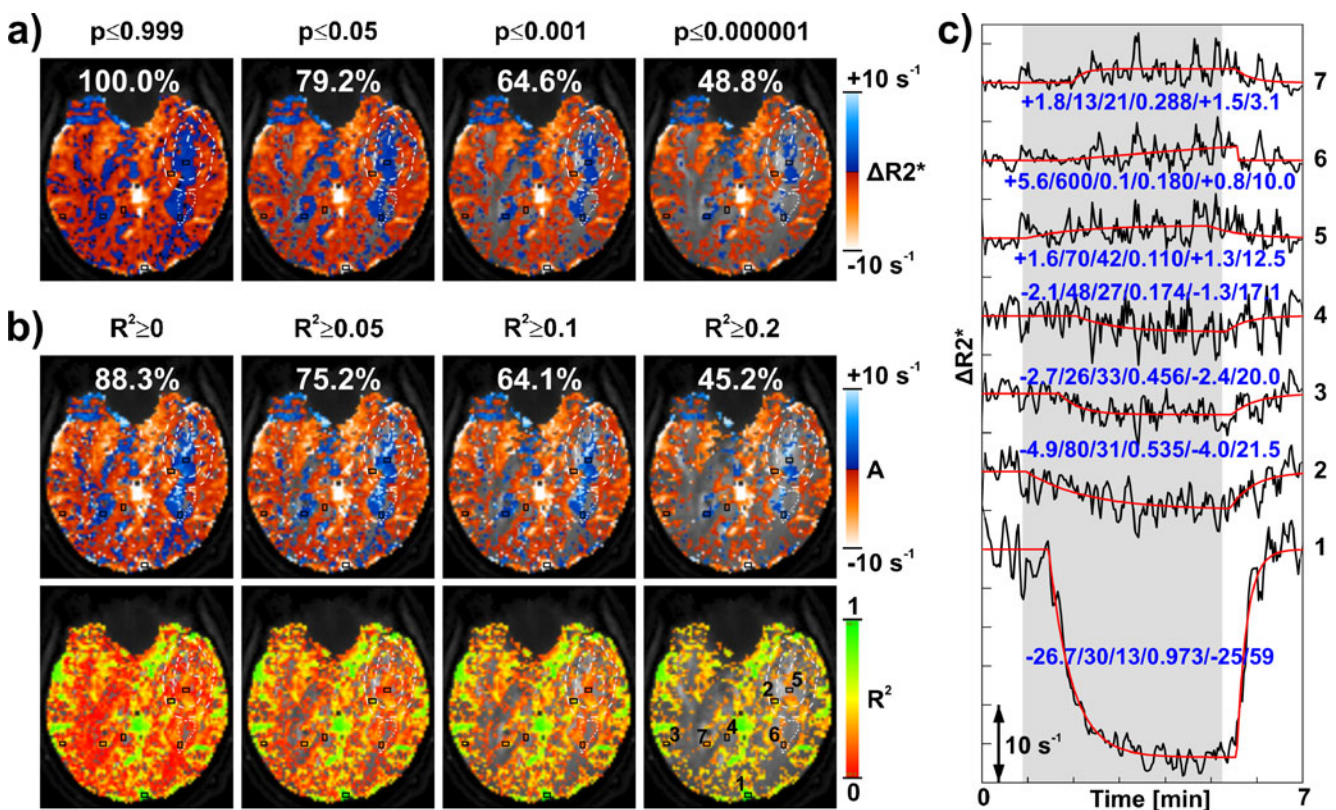


**Fig. 3** Results of voxel-wise response modelling (patient 4). Maps of maximum change  $A$  and fit quality  $R^2$  for different thresholds of  $R^2$  values (b) are displayed in comparison with the  $\Delta R2^*$  maps for different thresholds of the significance level  $p$  (a). For each map the number of responsive voxels is given as a percentage of the total number of voxels within this brain area. Examples of response functions for voxels placed in the superior sagittal sinus (1), ‘contrast-enhancing’ tumour region (2), grey matter (3), white matter (4),

‘necrosis’ (5), ‘oedema’ (6), and liquor (7) are given in c) together with the fit results (maximum change  $A$  [ $\text{s}^{-1}$ ] /  $\tau_1$  [s] /  $\tau_2$  [s] /  $R^2$  /  $\Delta R2^*$  [ $\text{s}^{-1}$ ] / baseline  $R2^*$  [ $\text{s}^{-1}$ ]). The principal patterns of the changes look very similar on both maps,  $\Delta R2^*$  and  $A$ . However, outliers (white spots) impact the A-maps even for high  $R^2$  thresholds. On the other hand, the averaging over the response period as performed for the  $\Delta R2^*$  maps might result in underestimation of the response amplitude

**Table 6** Comparison between the type of R2\* response and the perfusion grade. For each defined ROI (Fig. 1), the perfusion grade is compared with the predominant type of R2\* response obtained from

Patient	Tumour			Necrosis			Oedema		
	CASL	$\Delta R2^*(\text{Carbogen})$	$\Delta R2^*(\text{CO}_2/\text{air})$	CASL	$\Delta R2^*(\text{Carbogen})$	$\Delta R2^*(\text{CO}_2/\text{air})$	CASL	$\Delta R2^*(\text{Carbogen})$	$\Delta R2^*(\text{CO}_2/\text{air})$
P1	hyper	n	n				hypo	n	p
P2	hypo	ns	ns						
P3	iso	n	n	hypo	ns	p	hypo	ns	ns
P4	hyper	n	n	iso	p	ns	hypo	p	p
P5	iso	n	n						
P6	iso	n	ns	hypo	p/ns	p	hypo	p	ns
P7	iso	ns	ns				hypo	p	ns

**Table 4.** The abbreviations ‘hyper’, ‘iso’, and ‘hypo’ denote hyper-, iso-, and hypoperfused areas, respectively. ‘n’, ‘p’, and ‘ns’ mean predominant negative, positive and non-significant R2\* change

with high temporal and spatial resolution at 3.0 T. This approach has been validated in volunteers [15].

In this study we made four key observations:

- (1) ‘Non-tumoral’ brain tissue of patients showed a consistent decrease in R2\* during both respiratory challenges. If compared to healthy subjects [15], the maximum changes of these responses were of the same size, but with larger interindividual variations, and the time constants,  $\tau_1$  and  $\tau_2$ , were up to two times larger. These differences may be attributed to changes in blood supply and oxygen consumption of the tumour during the respiratory challenge. Other factors may be the greater anatomical variation of the non-tumoral area due to the varying slice locations in patients as well as changes in vasoreactivity related to age differences, underlying vascular diseases or treatment with dexamethasone before surgery.
- (2) The R2\* response maps of human intracranial tumours showed heterogeneous distributions with large interindividual variability but some general patterns. Meningiomas showed a strong R2\* decrease in the ‘contrast-enhancing’ area or no response to both gases, which agrees with previous carbogen measurements [39]. In glioblastomas, metastases and the lymphoma, ‘contrast-enhancing’ areas revealed subareas

with increased, decreased and unchanged R2\* values for CO<sub>2</sub>/air and partly even for carbogen. A heterogeneous signal response in high-grade glioblastomas was also found in [37]. We generally observed increased or unchanged R2\* values in necrotic areas and perifocal oedemas. In CSF spaces increased R2\* values during both respiratory challenges were also found but the mechanism still needs further elucidation [26].

- (3) The response characteristic was independent of contrast enhancement and perfusion. Hyperperfused tumour areas preferentially responded with negative R2\* changes to both respiratory challenges. All types of responses were found in ‘contrast-enhancing’ areas and in iso- and hypoperfused areas. Animal studies have shown that vascular maturation/vasoreactivity and permeability do not spatially overlap [29]. In human brain tumours, other than in healthy tissue, no correlation has been found between BOLD signal intensity changes during oxygen inhalation and the cerebral blood volume [38].
- (4) The temporal behaviour of the tumour response differed in some cases strongly from the normal response in healthy tissue, which is challenging for response modelling. Motivated by the good results in healthy tissue [15], a fit of a monoexponential model function was performed in this study. A good fit quality was reached for negative responses in ‘non-tumoral’ tissue and in most of the ‘contrast-enhancing’ tumour areas. However, in other tumour areas, especially in areas of necrosis and oedema, the R2\* time series exhibited relevant temporal variations resulting in low fit quality. In some of the investigated tumour areas remarkable long time constants were observed. However, in 90% of the ROI response functions more than 92% of the maximum change was reached at the end of the response/normalisation period. This confirms an appropriate choice of the breathing cycle durations. The detection sensitivity

**Table 7** For each grade of perfusion, the total numbers of ROIs with predominantly negative, positive and non-significant R2\* change are listed

CASL	$\Delta R2^*(\text{Carbogen})$			$\Delta R2^*(\text{CO}_2/\text{air})$		
	n	p	ns	n	p	ns
hyper	2	–	–	2	–	–
iso	3	1	1	2	–	3
hypo	1	4	4	–	4	4

achieved in ‘non-tumoral’ tissue in this study compared favourably with the assessment in healthy volunteers [15]. Nearly the same amount of significantly changed voxels were reached: 74(3)% vs 76(8)% for carbogen, 66(9)% vs 65(8)% for CO<sub>2</sub>/air in patients and volunteers, respectively.

The interpretation of R2\* changes in tumours is complex. In normal cerebral tissue, oxygenation saturation and cerebral blood flow increase during hyperoxia and hypercapnia resulting in a decrease of R2\*. This ‘normal’ response requires healthy blood vessels but may still be observed in mature tumour vessels [28]. Abnormal tumour vessels arising from angiogenesis with different architecture and lack of smooth muscles will lead to different R2\* response behaviour. The lack of vasoreactivity of immature vessels may lead to a lack of R2\* response during CO<sub>2</sub>/air inhalation [46]. The absence of any response to both gases may occur in areas with low blood volume or haematocrit [47], or in areas with high blood oxygenation saturation. Increased R2\* values may be found in areas with reduced blood flow related to vascular steal, increased blood volume, or reduced blood pH (Bohr effect) [18].

Accompanied measurements such as cerebral blood volume/flow during CO<sub>2</sub>/air inhalation or R1 relaxation rate during carbogen inhalation [48] may complement the assessment of R2\*. In this work we favoured the investigation of two different inhalation gases. Using CO<sub>2</sub>/air together with carbogen offers the possibility of differentiating between R2\* changes due to increased oxygenation and those related to vasoreactivity. Such information regarding tumour vessel function and maturity is beyond standard MRI and may complement a multi-modal approach of tumour characterisation, treatment planning and monitoring: e.g. improved oxygenation during carbogen inhalation may allow better selection of patients who benefit from hyperoxia modulation therapies such as ARCON therapy [49], the assessment of vessel maturation may impact on monitoring novel anti-angiogenetic or anti-vascular treatments and provides complementary information to contrast-enhanced MRI parameters [27, 29] and the derived volumetric measurements of tumour growth [50].

Our study is limited by the small and heterogeneous patient group. We sought to demonstrate the feasibility and robustness of the proposed method prior to addressing one specific tumour entity. A clinical limitation may arise from the acquisition of only one slice. However, dense sampling of the response curve in one slice maximises the statistical power of the experiment and enables the modelling of the R2\* response. Further studies are needed to better define typical patterns in different tumour entities and to determine the potential role of this method in therapy planning and monitoring. An intra-operative correlation [51] and a direct

comparison with histopathology in specific tumour regions would improve the understanding of the measured R2\* changes.

In the present study we demonstrated the feasibility of mapping the R2\* response of intracranial human tumours to hyperoxic and hypercapnic respiratory challenges. This measurement of oxygenation changes and vasoreactivity is non-invasive, does not involve ionising radiation, and provides information beyond standard anatomical and functional MRI.

## References

1. Yen PS, Teo BT, Chiu CH, Chen SC, Chiu TL, Su CF (2009) White Matter tract involvement in brain tumors: a diffusion tensor imaging analysis. *Surg Neurol* 72:464–469
2. Lu S, Ahn D, Johnson G, Law M, Zagzag D, Grossman RI (2004) Diffusion-tensor MR imaging of intracranial neoplasia and associated peritumoral edema: introduction of the tumor infiltration index. *Radiology* 232:221–228
3. Ludemann L, Warmuth C, Plotkin M, Forschler A, Gutberlet M, Wust P, Amthauer H (2009) Brain tumor perfusion: comparison of dynamic contrast enhanced magnetic resonance imaging using T1, T2, and T2\* contrast, pulsed arterial spin labeling, and H2(15)O positron emission tomography. *Eur J Radiol* 70:465–474
4. Zaharchuk G (2007) Theoretical basis of hemodynamic MR imaging techniques to measure cerebral blood volume, cerebral blood flow, and permeability. *AJNR Am J Neuroradiol* 28:1850–1858
5. Gerstner ER, Sorensen AG, Jain RK, Batchelor TT (2008) Advances in neuroimaging techniques for the evaluation of tumor growth, vascular permeability, and angiogenesis in gliomas. *Curr Opin Neurol* 21:728–735
6. Swanson KR, Chakraborty G, Wang CH, Rockne R, Harpold HL, Muzi M, Adamsen TC, Krohn KA, Spence AM (2009) Complementary but distinct roles for MRI and 18F-fluoromisonidazole PET in the assessment of human glioblastomas. *J Nucl Med* 50:36–44
7. Nehmeh SA, Lee NY, Schroder H, Squire O, Zanzonico PB, Erdi YE, Greco C, Mageras G, Pham HS, Larson SM, Ling CC, Humm JL (2008) Reproducibility of intratumor distribution of (18)F-fluoromisonidazole in head and neck cancer. *Int J Radiat Oncol Biol Phys* 70:235–242
8. Barrett T, Brechbiel M, Bernardo M, Choyke PL (2007) MRI of tumor angiogenesis. *J Magn Reson Imaging* 26:235–249
9. Padhani AR, Krohn KA, Lewis JS, Alber M (2007) Imaging oxygenation of human tumours. *Eur Radiol* 17:861–872
10. Baudalet C, Gallez B (2005) Current issues in the utility of blood oxygen level dependent MRI for the assessment of modulations in tumor oxygenation. *Curr Med Imaging Rev* 1:229–243
11. Neeman M, Dafni H (2003) Structural, functional, and molecular MR imaging of the microvasculature. *Annu Rev Biomed Eng* 5:29–56
12. Yetkin FZ, Mendelsohn D (2002) Hypoxia imaging in brain tumors. *Neuroimaging Clin N Am* 12:537–552
13. Ogawa S, Lee TM, Kay AR, Tank DW (1990) Brain magnetic resonance imaging with contrast dependent on blood oxygenation. *Proc Natl Acad Sci U S A* 87:9868–9872
14. Punwani S, Ordidge RJ, Cooper CE, Amess P, Clemence M (1998) MRI measurements of cerebral deoxyhaemoglobin concentration [dHb]—correlation with near infrared spectroscopy (NIRS). *NMR Biomed* 11:281–289



15. Mürtz P, Flacke S, Müller A, Soehle M, Wenningmann I, Kovacs A, Träber F, Willinek WA, Gieseke J, Schild HH, Remmele S (2010) Changes in the MR relaxation rate  $R2^*$  induced by respiratory challenges at 3.0 T: a comparison of two quantification methods. *NMR Biomed* doi:10.1002/nbm.1532
16. Ashkanian M, Borghammer P, Gjedde A, Istergaard L, Vafaee M (2008) Improvement of brain tissue oxygenation by inhalation of carbogen. *Neuroscience* 156:932–938
17. Baudelet C, Gallez B (2002) How does blood oxygen level-dependent (BOLD) contrast correlate with oxygen partial pressure ( $pO_2$ ) inside tumors? *Magn Reson Med* 48:980–986
18. Howe FA, Robinson SP, McIntyre DJ, Stubbs M, Griffiths JR (2001) Issues in flow and oxygenation dependent contrast (FLOOD) imaging of tumours. *NMR Biomed* 14:497–506
19. Heyn C, Poubanc J, Crawley A, Mandell D, Han JS, Tymianski M, Terbrugge K, Fisher JA, Mikulis DJ (2010) Quantification of Cerebrovascular Reactivity by Blood Oxygen Level-Dependent MR Imaging and Correlation with Conventional Angiography in Patients with Moyamoya Disease. *AJNR Am J Neuroradiol* 31:862–867
20. Goode SD, Krishan S, Alexakis C, Mahajan R, Auer DP (2009) Precision of cerebrovascular reactivity assessment with use of different quantification methods for hypercapnia functional MR imaging. *AJNR Am J Neuroradiol* 30:972–977
21. Yezhuvath US, Lewis-Amezcuca K, Varghese R, Xiao G, Lu H (2009) On the assessment of cerebrovascular reactivity using hypercapnia BOLD MRI. *NMR Biomed* 22:779–786
22. Ziyeh S, Rick J, Reinhard M, Hetzel A, Mader I, Speck O (2005) Blood oxygen level-dependent MRI of cerebral  $CO_2$  reactivity in severe carotid stenosis and occlusion. *Stroke* 36:751–756
23. van der Zande FH, Hofman PA, Backes WH (2005) Mapping hypercapnia-induced cerebrovascular reactivity using BOLD MRI. *Neuroradiology* 47:114–120
24. Kastrup A, Kruger G, Neumann-Haefelin T, Moseley ME (2001) Assessment of cerebrovascular reactivity with functional magnetic resonance imaging: comparison of  $CO_2$  and breath holding. *Magn Reson Imaging* 19:13–20
25. Vesely A, Sasano H, Volgyesi G, Somogyi R, Tesler J, Fedorko L, Grynszpan J, Crawley A, Fisher JA, Mikulis D (2001) MRI mapping of cerebrovascular reactivity using square wave changes in end-tidal  $PCO_2$ . *Magn Reson Med* 45:1011–1013
26. Rostrup E, Law I, Blinkenberg M, Larsson HB, Born AP, Holm S, Paulson OB (2000) Regional differences in the CBF and BOLD responses to hypercapnia: a combined PET and fMRI study. *NeuroImage* 11:87–97
27. Baudelet C, Cron GO, Gallez B (2006) Determination of the maturity and functionality of tumor vasculature by MRI: correlation between BOLD-MRI and DCE-MRI using P792 in experimental fibrosarcoma tumors. *Magn Reson Med* 56:1041–1049
28. Neeman M, Dafni H, Bukhari O, Braun RD, Dewhirst MW (2001) In vivo BOLD contrast MRI mapping of subcutaneous vascular function and maturation: validation by intravital microscopy. *Magn Reson Med* 45:887–898
29. Gilad AA, Israely T, Dafni H, Meir G, Cohen B, Neeman M (2005) Functional and molecular mapping of uncoupling between vascular permeability and loss of vascular maturation in ovarian carcinoma xenografts: the role of stroma cells in tumor angiogenesis. *Int J Cancer* 117:202–211
30. Baudelet C, Ansiaux R, Jordan BF, Havaux X, Macq B, Gallez B (2004) Physiological noise in murine solid tumours using  $T2^*$ -weighted gradient-echo imaging: a marker of tumour acute hypoxia? *Phys Med Biol* 49:3389–3411
31. Rodrigues LM, Howe FA, Griffiths JR, Robinson SP (2004) Tumor  $R2^*$  is a prognostic indicator of acute radiotherapeutic response in rodent tumors. *J Magn Reson Imaging* 19:482–488
32. Landuyt W, Hermans R, Bosmans H, Sunaert S, Beatse E, Farina D, Meijerink M, Zhang H, Van Den BW, Lambin P, Marchal G (2001) BOLD contrast fMRI of whole rodent tumour during air or carbogen breathing using echo-planar imaging at 1.5 T. *Eur Radiol* 11:2332–2340
33. Abramovitch R, Dafni H, Smouha E, Benjamin LE, Neeman M (1999) In vivo prediction of vascular susceptibility to vascular susceptibility endothelial growth factor withdrawal: magnetic resonance imaging of C6 rat glioma in nude mice. *Cancer Res* 59:5012–5016
34. Robinson SP, Collingridge DR, Howe FA, Rodrigues LM, Chaplin DJ, Griffiths JR (1999) Tumour response to hypercapnia and hyperoxia monitored by FLOOD magnetic resonance imaging. *NMR Biomed* 12:98–106
35. Kuperman VY, River JN, Lewis MZ, Lubich LM, Karczmar GS (1995) Changes in  $T2^*$ -weighted images during hyperoxia differentiate tumors from normal tissue. *Magn Reson Med* 33:318–325
36. Sedlacik J, Kutschbach C, Rauscher A, Deistung A, Reichenbach JR (2008) Investigation of the influence of carbon dioxide concentrations on cerebral physiology by susceptibility-weighted magnetic resonance imaging (SWI). *NeuroImage* 43:36–43
37. Rauscher A, Sedlacik J, Fitzek C, Walter B, Hochstetter A, Kalff R, Kaiser WA, Reichenbach JR (2005) High resolution susceptibility weighted MR-imaging of brain tumors during the application of a gaseous agent. *Röfo* 177:1065–1069
38. Losert C (2004) Sauerstoff-induzierte Signaländerungen in der MRT von Hirntumoren. Dissertation. University of Munich, Germany
39. Rijpkema M, Schuurin J, Bernsen PL, Bernsen HJ, Kaanders JH, van der Kogel AJ, Heerschap A (2004) BOLD MRI response to hypercapnic hyperoxia in patients with meningiomas: correlation with Gadolinium-DTPA uptake rate. *Magn Reson Imaging* 22:761–767
40. Rijpkema M, Kaanders JH, Joosten FB, van der Kogel AJ, Heerschap A (2002) Effects of breathing a hyperoxic hypercapnic gas mixture on blood oxygenation and vascularity of head-and-neck tumors as measured by magnetic resonance imaging. *Int J Radiat Oncol Biol Phys* 53:1185–1191
41. Taylor NJ, Baddeley H, Goodchild KA, Powell ME, Thoumine M, Culver LA, Stirling JJ, Saunders MI, Hoskin PJ, Phillips H, Padhani AR, Griffiths JR (2001) BOLD MRI of human tumor oxygenation during carbogen breathing. *J Magn Reson Imaging* 14:156–163
42. Griffiths JR, Taylor NJ, Howe FA, Saunders MI, Robinson SP, Hoskin PJ, Powell ME, Thoumine M, Caine LA, Baddeley H (1997) The response of human tumors to carbogen breathing, monitored by Gradient-Recalled Echo Magnetic Resonance Imaging. *Int J Radiat Oncol Biol Phys* 39:697–701
43. Remmele S, Dahnke H, Flacke S, Soehle M, Wenningmann I, Kovacs A, Träber F, Müller A, Willinek WA, König R, Clusmann H, Gieseke J, Schild HH, Murtz P (2010) Quantification of the magnetic resonance signal response to dynamic (C)O<sub>2</sub>-enhanced imaging in the brain at 3 T:  $R2^*$  BOLD vs. balanced SSFP. *J Magn Reson Imaging* 31:1300–1310
44. Peebles K, Celi L, McGrattan K, Murrell C, Thomas K, Ainslie PN (2007) Human cerebrovascular and ventilatory  $CO_2$  reactivity to end-tidal, arterial and internal jugular vein  $PCO_2$ . *J Physiol* 584:347–357
45. Hsu YY, Chang CN, Jung SM, Lim KE, Huang JC, Fang SY, Liu HL (2004) Blood oxygenation level-dependent MRI of cerebral gliomas during breath holding. *J Magn Reson Imaging* 19:160–167
46. Packard SD, Mandeville JB, Ichikawa T, Ikeda K, Terada K, Niloff S, Chiocca EA, Rosen BR, Marota JJ (2003) Functional response of tumor vasculature to  $PaCO_2$ : determination of total and microvascular blood volume by MRI. *Neoplasia* 5:330–338



47. Robinson SP, Rijken PF, Howe FA, McSheehy PM, van der Sanden BP, Heerschap A, Stubbs M, van der Kogel AJ, Griffiths JR (2003) Tumor vascular architecture and function evaluated by non-invasive susceptibility MRI methods and immunohistochemistry. *J Magn Reson Imaging* 17:445–454
48. O'Connor JP, Naish JH, Parker GJ, Waterton JC, Watson Y, Jayson GC, Buonaccorsi GA, Cheung S, Buckley DL, McGrath DM, West CM, Davidson SE, Roberts C, Mills SJ, Mitchell CL, Hope L, Ton NC, Jackson A (2009) Preliminary study of oxygen-enhanced longitudinal relaxation in MRI: a potential novel biomarker of oxygenation changes in solid tumors. *Int J Radiat Oncol Biol Phys* 75:1209–1215
49. Kaanders JH, Bussink J, van der Kogel AJ (2002) ARCON: a novel biology-based approach in radiotherapy. *Lancet Oncol* 3:728–737
50. Ertl-Wagner BB, Blume JD, Peck D, Udupa JK, Herman B, Levering A, Schmalfuss IM (2009) Reliability of tumor volume estimation from MR images in patients with malignant glioma. Results from the American College of Radiology Imaging Network (ACRIN) 6662 Trial. *Eur Radiol* 19:599–609
51. Schaller C, Schramm J, Haun D, Meyer B (2003) Patterns of cortical oxygen saturation changes during CO<sub>2</sub> reactivity testing in the vicinity of cerebral arteriovenous malformations. *Stroke* 34:938–944